Article

Role of Source, Mineralogy, and Organic Complexation on Lability and Fe Isotopic Composition of Terrestrial Fe sources to the Gulf of Alaska

Linqing Huang,* Sarah M. Aarons, Bess G. Koffman, Wenhan Cheng, Lena Hanschka, Lee Ann Munk, Jordan Jenckes, Emmet Norris, and Carli A. Arendt

Read Online

ACCESS | Metrics & More | Article Recommendations | SI Supporting Information

ABSTRACT: Iron (Fe) is a key trace nutrient supporting marine primary production, and its deposition in the surface ocean can impact multiple biogeochemical cycles. Understanding Fe cycling in the subarctic is key for tracking the fate of particulate-bound sources of oceans in a changing climate. Recently, Fe isotope ratios have been proposed as a potential tool to trace sources of Fe to the marine environment. Here, we investigate the Fe isotopic composition of terrestrial sources of Fe including glacial sediment, loess, volcanic ash, and wildfire aerosols, all from Alaska. Results show that the δ^{56}Fe values of glaciofluvial silt, glacial dissolved load, volcanic ash, and wildfire aerosols fall in a restricted range of δ^{56}Fe values from −0.02 to +0.12‰, in contrast to the broader range of Fe isotopic compositions observed in loess, −0.50 to +0.13‰. The Fe isotopic composition of the dissolved load of glacial meltwater was consistently lighter compared to its particulate counterpart.

The 'aging' (exposure to environmental conditions) of volcanic ash did not significantly fractionate the Fe isotopic composition. The Fe isotopic composition of wildfire aerosols collected during an active fire season in Alaska in the summer of 2019 was not significantly fractionated from those of the average upper continental crust composition. We find that the δ^{56}Fe values of loess (<5 μm fraction) were more negative (−0.32 to +0.05‰) with respect to all samples measured here, had the highest proportion of easily reducible Fe (5.9−59.6%), and were correlated with the degree of chemical weathering and organic matter content. Transmission electron spectroscopy measurements indicate an accumulation of amorphous Fe phases in the loess. Our results indicate that Fe isotopes can be related to Fe lability when in the presence of organic matter and that higher organic matter content is associated with a distinctly more negative Fe isotope signature likely due to Fe-organic complexation.

KEYWORDS: Fe isotopes, organic complexation, chemical weathering, biogeochemistry, volcanic ash
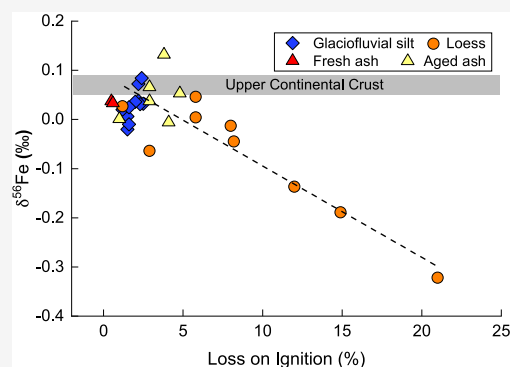
1. INTRODUCTION

The northeast subarctic Pacific Ocean is considered a high nutrient, low chlorophyll (HNLC) region. Severe iron (Fe) deficiency in this region limits phytoplankton growth and results in low levels of primary production, despite elevated macronutrient (nitrate, phosphate, and silicate) concentrations.[1] Phytoplankton are the base of the marine food web and can contribute to the sequestration of atmospheric carbon dioxide (CO_2), thus impacting the global carbon cycle.[2−7] Terrestrial nutrients delivered to the ocean are typically supplied through riverine sediment discharge and the atmospheric deposition of ash from volcanic eruptions and aeolian dust. Aerosols derived from combustion, biomass burning, and natural wildfire aerosols also contribute soluble Fe to the marine environment.[8−11] Particulate matter transported via wind in the atmosphere is more likely than the riverine discharge to reach beyond the continental shelf and thus can have a greater potential to impact the open ocean productivity.

As an essential trace nutrient, Fe is involved in numerous processes in the ocean, such as photosynthesis,[12] respiration,[13] and nitrogen fixation.[14] However, the concentration of Fe in the surface ocean is generally low. Even during the glacial melt months of April through August, the concentration of dissolved Fe in the Gulf of Alaska (GoA) ranges only from ~0.6 to 4.0 nmol/kg.[15] Numerous studies have demonstrated that Fe addition can stimulate primary production in HNLC ocean regions.[2−7] One proposed method for tracking the
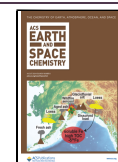
sources and bioavailability of Fe in the ocean is the use of stable Fe isotopic ratios. In the past two decades, Fe isotopic ratios have been widely utilized in studies of crust-mantle evolution, magmatic differentiation, hydrothermal processes, and cosmochemistry.[16−20] Recently, there has been a significant expansion in the number of studies utilizing Fe isotopes in the oceanic Fe cycle (see Fitzsimmons and Conway, 2023 for a detailed summary),[21] leading to major advances in identifying Fe sources and internal cycling processes such as speciation changes, biological uptake, and particle scavenging.[8,16,21−24] The Fe isotopic composition is expressed by δ^{56}Fe defined relative to the international reference material IRMM-014:

$$\delta^{56}\text{Fe} = 1000 \times [(^{56}\text{Fe}/^{54}\text{Fe})_{\text{sample}}/(^{56}\text{Fe}/^{54}\text{Fe})_{\text{IRMM−014}} - 1] \quad (1)$$

Dust and riverine sediments are typically characterized by δ^{56}Fe values that are close to the average Fe isotopic signature of the upper continental crust (δ^{56}Fe = +0.08 ± 0.04‰, 95% CI).[25,26] However, subglacial streams in southwestern Alaska have δ^{56}Fe values that trend toward more negative Fe isotope compositions (δ^{56}Fe = −1.7‰,) suggesting that dissolved riverine Fe in subglacial environments is isotopically light relative to the igneous rocks from which it erodes.[27] Similarly, the Fe isotopic compositions of the dissolved load and suspended sediment in the Lena River (Northeast Siberia) are isotopically lighter than the upper continental crust as a result of chemical weathering-induced fractionation.[28] It has been proposed that chemical weathering influences the Fe flux, solubility, and speciation of river sediments and dust sourced from glacial environments.[29−31] Moreover, previous studies show that the evolution of dissolved riverine Fe is often influenced by organic carbon (OC) during transport toward the coastal zone.[31] In general, the Fe isotopic composition of the dissolved fraction of glacial meltwaters is widely variable, with most variation attributed to biological fractionation within ice (e.g., sea ice in de Jong et al.).[32] Two primary forms of Fe compounds—Fe−OC and Fe oxyhydroxides—are typically found in the dissolved fraction. Stable Fe isotopes can be used to investigate chemical pathways for Fe and Fe bound to OC during weathering in boreal−estuarine regions, since Fe isotope fractionation may occur during incremental Fe(III)$_{\text{aq}}$ precipitation and Fe−OC complexation.[28,31,33,34]

The release of Fe from industrial combustion and biomass burning has also been recognized as an important source of bioavailable Fe to the surface oceans.[8−10,21,24,35,36] Iron sourced from industrial combustion is highly soluble, and model studies estimate that approximately 30% of atmospherically transported soluble Fe is from combustion sources.[37] The δ^{56}Fe isotopic composition of industrial combustion sourced Fe ranges up to 4‰ lower than that of natural Fe,[24] which suggests that Fe isotopes have the potential to fingerprint different sources of aerosol Fe.[8,24] Low Fe isotopic compositions have been observed in plants (δ^{56}Fe = −1.64 to +0.17‰),[38,39] however, particulates sourced from wildfire events contain substantial soil-derived material which may drive the Fe isotopic compositions of wildfire aerosols to be closer to soil or crustal values.[40] The Fe isotopic composition of this type of biomass-burning aerosol is still relatively unconstrained.

Here, we investigate the Fe isotope compositions of several important potential Fe sources, including glaciofluvial silt and dissolved load, loess, fresh and aged volcanic ash, and natural wildfire aerosols. The goal is to establish Fe isotopic signatures of these terrestrial Fe sources to the Gulf of Alaska (GoA) and to explore the effects of the formation mechanism (e.g., glaciogenic, volcanic, and transport/storage) and process (e.g., aeolian, fluvial, chemical weathering, and coincident with organic matter) on the Fe geochemistry and lability. In addition, we use transmission electron spectroscopy to gain insight into the mineralogical and/or weathering controls on the measured Fe isotopic compositions of glaciofluvial silt and loess samples studied here.

2. SAMPLES AND METHODOLOGY

2.1. Sampling Locations and Description. *2.1.1. Loess Sampling and Size Separation.* Loess is fine-grained wind-blown sediment resulting from the grinding of regolith by ice sheets and glaciers or through wind abrasion of sediments, which is then preserved in sedimentary layers that can be tens to hundreds of meters thick. Dust formed by glacial abrasion can be carried beyond the most advanced glacier positions in glaciofluvial outwash, uplifted by wind, and deposited as loess.[41,42] Glacial loess serves as a paleoclimate archive used to investigate Fe availability and transport and to gauge potential carbon cycle impacts in high-latitude environments on glacial-interglacial timescales.[41,43,44] In modern environments, glaciogenic dust may play an important role in the overall global dust budget, particularly with respect to Fe delivery to the northeastern subarctic Pacific Ocean, which is Fe-limited.[15,31,45,46] Active dust transport from glacial catchments, evidenced by the accumulation of loess at downwind sites, occurs throughout southcentral Alaska.[42,44]

We measured the Fe isotopic composition of nine loess samples collected from the Chitina, Matanuska, and Copper River valleys, including some previously studied samples.[43] The Chitina loess section in the Copper River Valley has the highest mass accumulation rates for the fine-grained (<20 μm) fraction reported for high-latitude regions of the Northern Hemisphere during the Holocene.[41] Radiocarbon dates, mineralogy, and geochemistry of the Chitina loess section indicate the accumulation of dust over the past ~10,000 years.[41] The loess samples from the Copper River Valley, Chitina River Valley, and the Matanuska River Valleys are hereafter referred to as the river valley loess. Six additional loess samples were collected from ~20 m of exposed Pleistocene aeolian deposits from Kanakanak bluffs, located in the Nushagak lowlands near Bristol Bay, Alaska (hereafter referred to as KNK loess). These sediments are dominated by the coarse fraction (30−63 μm) and are described as sand-sheet deposits and sand-loess intergrades.[47] The "sandy loess" deposit reflects a very fast aeolian deposition rate after subsequent ice melt following the deglaciation from the Last Glacial Period.[47]

2.1.2. Glacial River Sampling and Filtration. Rivers play an important role in regulating the flux, concentration, and bioavailability of Fe in surface oceans. The boreal zone of glacierized systems in Alaska and Greenland is experiencing rapid climate and environmental change, and glaciofluvial sediments exert an increasing influence on Fe geochemistry in high-latitude oceans.[27,31,48] The input of glaciofluvial Fe varies seasonally, usually peaking during snowmelt in spring and glacial melt in summer.[15]

Sediment was sampled from several rivers draining alpine glaciers in southcentral Alaska and the Yukon Territory in

Canada in the summers of 2016 and 2017 to assess the spatial and seasonal variations in input and speciation of Fe delivered to the GoA.[43] Samples were collected either from river channel deposits or along riverbanks downstream from source glaciers. Eleven glaciofluvial silts were collected in 2016 from the Matanuska, Susitna, Knik, Chistochina, Copper, and Gakona rivers,[43] whose watersheds cover a large region of Alaska, draining the Alaska, Talkeetna, Wrangell, and Chugach Mountains (see Table S1 for all sampling locations). Glacier meltwater samples (dissolved load and suspended particulate matter) were also collected during the summer melt season from the Matanuska River in 2019 and the Tutka River and Grewingk River in the summer of 2021 (locations in Figure 1
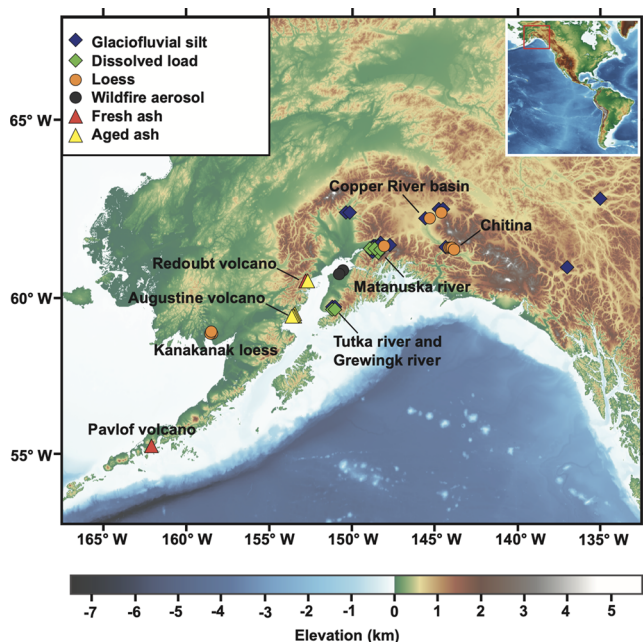
Figure 1. Map indicating the locations of samples analyzed in this study, including from southcentral Alaska, USA, and Yukon Territory, Canada. Map generated using GMTApp. The sample sites of suspended particulate are the same as those of dissolved load.

and Table S1). Sampling bottles (LDPE Nalgene) were washed in a soap detergent mixture overnight at 60 °C, followed by a 48-h leach in 10% HNO_3 (trace-metal grade) at room temperature, rinsed with MilliQ water, followed by a 48-h leach in 10% HCl (optima grade) at room temperature, and a final rinse with MilliQ water consistent with previously described methods for field collection for Fe isotopic composition of glacial meltwater.[30] Following water collection, these samples were immediately filtered through acid-precleaned 0.2 μm PTFE filters and acidified to pH 1.7−1.8 using HCl (optima grade).[30] The sampling protocol follows established trace-metal clean methods to avoid ultratrace level metal contamination (e.g., Fe, U, Hf, and Nd).[30,49] Field blanks were collected using the same filtration and acidification procedure with MilliQ water and field blank concentrations are reported in Section 2.2.4. The filtered water samples were evaporated in an ISO Class 7 exhausted laminar flow hood and processed for sample digestion and column chemistry as described below.

2.1.3. Volcanic Ash. Volcanic ash has been increasingly recognized as a source of Fe to the surface ocean.[50,51] Volcanic eruptive plumes typically include a mixture of rock, mineral,

and glass particles, some of which are highly reactive and contain highly soluble Fe.[52,53] Volcanic ash may be ejected up to tens of kilometers into the atmosphere and the finest grains can be retained in the atmosphere for several days to weeks, allowing them to reach the open ocean. For example, the Aleutian volcanic chain in Alaska typically experiences explosive Plinian eruptions with ash reaching altitudes of 8500 m.a.s.l., depositing material hundreds to thousands of kilometers away.[54] Ash from volcanoes can release substantial amounts of macro- and micronutrients such as PO_4^{3-}, Si, Fe, Zn, Mn, Ni, Co, and Cu within 1−2 h of the eruption, significantly raising the surface ocean concentrations,[55−57] and its deposition can affect marine primary production through rapid Fe-release in contact with seawater. Following the eruption of the Kasatochi volcano in August 2008, a phytoplankton bloom in the subarctic northeast Pacific was detected by satellite observations[58] demonstrating how major volcanic eruptions can influence ocean surface nutrient fertilization.[59]

We examined volcanic ash samples provided by the U.S. Geological Survey (USGS) Alaska Volcano Observatory to investigate the Fe isotopic compositions of tephra from two volcanic eruptions within this volcanically active region. Two never-wetted fresh ash samples from the explosive Redoubt Volcano 2009 eruption and Pavlof Volcano 2016 eruption were collected to assess their Fe isotopic composition. In addition, six aged ash samples collected from a surface pit in a coastal bluff on Augustine Island were evaluated. The aged samples extend from 1989 A.D. to ~8700 years ago.[43,60,61] The fresh ash sample AT-3982 had a volume mode diameter of ~10−11 μm. Two aged ash samples, AT-2876 and AT-2886, had volume mode diameters of ~20 μm.[43]

2.1.4. Wildfire Aerosols from Forest Fires. Aerosols sourced from wildfire biomass burning are becoming a recognized source of Fe delivered to the open ocean.[36,62] We hereafter refer to these as wildfire aerosols. Atmospheric chemical transport models suggest that wildfire aerosols contribute a large fraction of labile Fe to the Southern Hemisphere, which can trigger widespread phytoplankton blooms in the Southern Ocean.[36,62] These studies suggest that wildfire aerosols may play an important role in the modulation of primary production in the surface ocean due to their enhanced Fe solubilities.

In the present study, two wildfire-sourced particulate samples from southcentral Alaska were collected using an active air sampler on PTFE filters from Eagle River, Alaska in 2019 (August 19 and August 25, during a wildfire event) by the Alaska Department of Environmental Conservation. Both samples consist of particles less than 10 μm in diameter (PM 10) and the sample site was located in very close proximity and downwind of the wildfire activity. By analyzing these two samples, we can establish a basic understanding of the δ^{56}Fe signature of wildfire aerosols in this region.

2.2. Sampling Methods and Analysis. *2.2.1. Reagents, Labware Cleaning and Blanks.* Laboratory work was carried out within class 100 laminar flow workstations in several laboratories, including the Climate & Earth Surface Geochemistry (CESG) clean laboratories at Scripps Institution of Oceanography (SIO), the Colby Lab for Ice and Climate at Colby College, and the Metal Stable Isotope Geochemistry lab at the University of Science and Technology of China (USTC). Chemical reagents to process the samples included MilliQ ultrapure water, in-house double-distilled HCl and

HNO$_3$, and Optima grade HF, HClO$_4$, and H$_2$O$_2$. Blank values for the undiluted stock acids are reported in Table S2 and are all below 0.02 ng Fe per mL of acid. All vials used for the sample collection and processing were acid-cleaned to minimize blanks, and no unexpected or unusually high safety hazards were encountered.

2.2.2. Sample Preparation. In total, 11 glaciofluvial silt, 19 suspended particulate matter, 8 dissolved load, 15 loess, 2 fresh volcanic ash, and 6 aged volcanic ash samples were analyzed for Fe isotopic compositions. As described in Koffman et al.,[43] all glaciofluvial silts, loess samples, and aged volcanic ashes were first separated by size. Bulk samples were passed through 63 μm sieves to remove all woody debris and whole rock materials (i.e., pebbles, coarse ash grains) that could not be removed in the field. Excluding loess from Kanakanak bluffs, particles <5 μm diameter were separated using wet sedimentation for glaciofluvial silt and loess samples, as the <5 μm fraction represents the material most likely to be wind-transported and contains more Fe-bearing clay minerals and Fe oxides, such as hematite, goethite, and chlorite.

Carbonates were removed using AcOH following the size separation and were only observed to be present in the Chitina loess section. We acknowledge that the samples analyzed here for Fe isotopic compositions do not include the carbonate fraction, and there may be some associated mass-dependent isotope fractionation during leaching (e.g., Revels et al.).[63] We expect the leachate to consist of the easily leachable portion such as the carbonate fraction, which should be minor compared to the amount of Fe hosted in the silicate and hydroxide portions of our loess samples. The mineralogy of samples was determined using X-ray diffractometry (XRD) at Colby College.[43] For these analyses, the <5 μm grain size fraction of sediment samples was analyzed, while bulk samples were used for the never-wetted volcanic ash. We also analyzed an additional six loess samples from Kanakanak bluffs which were separated into three size fractions, fine: 0.2−10 μm; medium: 10−30 μm; and coarse: 30−63 μm using precleaned PTFE filters to investigate potential variations in Fe isotopic composition with respect to size.

The loss on ignition (LOI) method was employed in this study for estimating the organic carbon (OC) content of loess samples. The nine fine-grained loess samples (<5 μm fraction) and six Kanakanak bluff loess samples (bulk) were added to ceramic crucibles, placed in an oven at 110 °C for 6 h, and then cooled and weighed to determine the water content. Subsequently, dried samples were ashed at 550 °C for 4 h, then cooled to room temperature and weighed. The LOI data are reported as the percent difference between the oven-dry (110 °C) loess mass and the loess mass after combustion (550 °C), divided by the oven-dry soil mass.

Sequential Fe extraction techniques were used to separate different Fe species including exchangeable, easily reducible, reducible, sheet silicates, and refractory fractions.[43,64] Sediment extractions were performed with a sample size of 100 mg. First, sediments were subjected to 10 mL of 1 M MgCl$_2$ at pH 7 for 2 h to extract exchangeable Fe(II) ions.[64−66] Next, 10 mL of 1 M hydroxylamine−hydrochloride solution was added in 25% v/v acetic acid to extract "easily reducible" Fe oxides (e.g., ferrihydrite and lepidocrocite).[64,65] Samples were placed on a rocking table for 24 h under dark conditions. The third extraction added sodium dithionite solution (50 g L$^{−1}$) buffered to pH 4.8 with acetic acid, sodium citrate, and sodium bicarbonate to extract "reducible" Fe oxides (e.g.,

goethite and hematite).[64,67,68] The organic carbon-associated Fe was completely leached out at this step.[43,67] Finally, samples were heated with 3 mL of 6 M HCl at 100 °C in Teflon beakers for 2 h for the extraction of Fe (hydr)oxides, siderite and ankerite, and Fe from certain sheet silicate minerals (e.g., nontronite, chlorite, glauconite, biotite).[64] Finally, the remaining portion of sediment was dissolved using a 1:3 ratio of concentrated HF-HNO$_3$ to determine the residual fraction of Fe.[43] Samples were diluted and acidified to 3% v/v HNO$_3$ prior to analysis. Procedural blank concentrations for sequential leaching were negligible, and no blank corrections were performed.[43]

After samples were separated by size, an aliquot of 100 mg of each sample powder was digested separately, following procedures established by previous work.[43,69,70] Dried samples were weighed into clean Savillex Teflon beakers, dissolved in an acid mixture of concentrated HNO$_3$ and concentrated HF in a 3:1 ratio, disaggregated in an ultrasonic bath for 20 min, and then capped and heated at 100 °C for >24 h. The sample powders were treated with 0.3−0.5 mL of concentrated HClO$_4$ followed by fuming at 200 °C to eliminate the organic matter. After evaporation to dryness, samples were treated twice successively with 6 mL of 8 M HNO$_3$ followed by 20 min in an ultrasonic bath and >1 h heating, capped, at 100 °C to remove residual halides. Dried, digested samples were finally redissolved in 5 mL of 4 M HNO$_3$. Aliquots for analysis were diluted to 3% v/v HNO$_3$.

Following the complete digestion, major and trace element concentrations were determined. Major element concentrations in digested and extracted samples were determined using a Spectro Arcos ICP-AES housed at Colby College.[43] Trace element concentrations were measured on a Thermo Finnigan Element II high-resolution ICP-MS at the University of Maine.[43] Procedural blank concentrations were negligible (<10 ng mL$^{−1}$), and standard concentrations were consistent with reported reference values. Additional information on analytical accuracy and precision can be found in Koffman et al.[43]

2.2.3. Fe Purification/Ion Exchange Chromatography. Digested samples provided nearly 70 μg Fe for isotopic analysis. The Fe purification was conducted in the clean laboratories at SIO and USTC. In summary, Fe was separated using chromatographic columns following a method[71,72] designed to provide sufficient isolation of Fe from major elements (Al, K, Na, Ca, Mg) within the sample matrix and from Cr, which has direct isobaric interferences on ^{54}Fe from ^{54}Cr. The column chemistry utilized a Poly-Prep column obtained from Bio-Rad (USA). This column can hold up to 0.5 mL of resin and has a 2 mL reservoir. Anionic chloride resin from Bio-Rad AG 1-X8 (200−400 mesh size) from Bio-Rad was used for the chemical purification of Fe. Digested samples were redissolved in 6 M HCl and loaded into the columns. The full procedural steps for this portion of the chemistry are provided in previous literature.[71−73] After column purification, samples were evaporated to dryness, redissolved, and diluted to 1.5 ppm in 2% (m/m) HNO$_3$ prior to elemental and isotopic analysis. The Fe yields were carefully checked to ensure that the chemical procedure achieved high recovery rates (>99%).

2.2.4. Mass Spectrometry. Iron isotope analysis of all samples was conducted using the Thermo Scientific Neptune Plus multicollector inductively coupled plasma mass spectrometer (MC-ICP-MS) at the Origins Lab at the University of Chicago and the Soil and Environment Analysis Center at the Institute of Soil Science, Chinese Academy Sciences. Sample

solutions were introduced into the instrument using nickel H and jet cones, an ESI PFA microflow nebulizer with an aspiration rate of ~50 μL min^{-1}, and a quartz dual cyclonic spray chamber. Measurements were performed in either medium or high mass resolution mode. Potential isobaric interferences from Cr and Ni were monitored at masses $^{53}Cr^+$ and $^{64}Ni^+$ and subtracted from Fe signals as necessary.[74] On-peak zero was determined by measurement of a pure 2% HNO_3 blank solution at the beginning of each analytical session and was subtracted from all standard and sample data. Instrumental mass fractionation was corrected using the sample-standard bracketing method.[74]

Each Fe isotope data analysis involved 60 cycles of 2.097 s integrations for each cycle, and baseline calibration occurred prior to each analysis. Samples were bracketed by measurements of IRMM-014 at the Soil and Environment Analysis Center and IRMM-524a (from which IRMM-014 is prepared) at the Origins Lab to account for the stability of the instrument for the highest quality control. These two standard materials have a Fe isotopic composition that is identical within analytical uncertainty.[74]

To avoid cross-contamination, 5% and 2% HNO_3 (m/m) were used for washing for at least 4 min between each measurement, until the ^{56}Fe signal was less than 3 mV. The total procedural blanks (from sample collection/dissolution to instrumental analysis) were <40 ng, which is negligible compared with the amount of Fe extracted from each sample (51−191 μg). Each sample was typically measured three or nine times nonsequentially during an analytical session.[73−75] The long-term precision of the isotopic compositions was 0.04‰ (95% CI) for $\delta^{56}Fe$, which is calculated based on repeated measurements of the IRMM-014 standard, and is adopted for uncertainty bars in the figures. We analyzed U.S. Geological Survey (USGS) rock standard BCR-2 as a random sample, and measured $\delta^{56}Fe$ = +0.089‰ ± 0.042 (95% CI, n = 3), in agreement with other reported literature values (e.g., $\delta^{56}Fe$ = +0.091 ± 0.017‰).[74]

2.2.5. TEM Imaging and Analyses. We analyzed Fe-bearing minerals in glaciofluvial silt and loess samples with Transmission Electron Microscopy (TEM) to identify the speciation and coordination of Fe. Dried silt and loess samples (<5 μm) were thinned from a micro to nanoscale using the Focused Ion Beam (FIB) method, which has proven to be extremely useful for preparing cross-sectional samples for TEM investigations.[76] The TEM grid samples were examined with a JEOL JEM-2800 field emission high-resolution TEM equipped with dual 100 μm^2 Silicon Drift Detectors for rapid EDS mapping at the UC Irvine Materials Research Institute. This microscope was also equipped with a Gatan Oneview camera that allows data capture in both imaging and in situ mode. Approximately 3 areas of each sample were analyzed, and the images included here are representative of about 30 TEM images of particles in total.

3. RESULTS

Major and trace element concentrations, bulk mineralogy, and Fe sequential leaches of glaciofluvial silt, loess, and volcanic ash have been previously reported by Koffman et al.[43] None of the samples—excluding a small subset of the river valley loess samples (all <5 μm size fraction)—show any variability in Fe isotopic composition with respect to Fe content (Figure S1).

The Fe isotopic compositions of wildfire aerosols, glaciofluvial silt, and volcanic ash span a relatively narrow

range of Fe isotopic compositions, with $\delta^{56}Fe$ = −0.10 to +0.12‰ (Figure 2 and Table S3). The loess spans a larger Fe
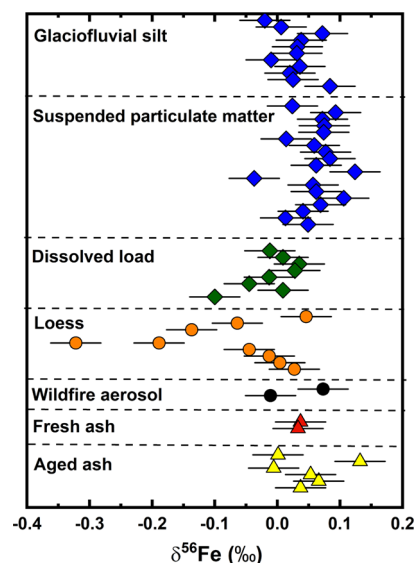
Figure 2. Stable Fe isotopic compositions of potential Fe sources to the Gulf of Alaska (note the loess shown here is only from the river valley loess profiles). Error bars show the 95% confidence intervals.

isotopic range, with $\delta^{56}Fe$= −0.50 to +0.13‰ (Figures 2 and 4). The lightest Fe isotopic compositions measured here, $\delta^{56}Fe$ = −0.32 and −0.50‰, were observed in the Chitina and Kanakanak bluff loess sections, respectively.

The LOI values of glaciofluvial silt, volcanic ash, and bulk KNK loess samples measured in this study span a narrow range from 0.5 to 2.5 wt %, whereas LOI in the loess samples from river valley spans a much larger range from 1.2 to 21 wt %. We found the LOI value of fine-grained loess to be negatively correlated to $\delta^{56}Fe$ isotopic composition (Section 4.3). The highest observed LOI value (21 wt %) measured in the Chitina loess samples corresponded to a very light Fe isotopic composition ($\delta^{56}Fe$ = −0.32‰).

4. DISCUSSION

4.1. Iron Isotope Compositions of Various Fe Reservoirs. *4.1.1. Volcanic Ash.* Though it is well recognized that volcanic ash is an important Fe source to the surface oceans, there have been few reports on the Fe isotopic compositions of volcanic ash, with the bulk of $\delta^{56}Fe$ values measured in bulk volcanic rocks ranging from −0.24 to +0.64‰.[25,77] Highly evolved granites with SiO_2 > 75 wt % have highly variable and sometimes very high $\delta^{56}Fe$ values (up to 0.64‰).[77] A recent study investigated the Fe isotopic composition of tephra layers, sediments, and mixed tephra-sediment samples, located offshore from the volcanically active island of Montserrat in the Caribbean Sea.[78] The fresh tephra deposited in Montserrat exhibited near-crustal $\delta^{56}Fe$ values ($\delta^{56}Fe$ = +0.02 ± 0.02‰, 2SD).[78] However, the buried tephra samples were found to have lower $\delta^{56}Fe$ values (down to −0.26‰),[78] reflecting the loss of isotopically heavier Fe during diagenesis.

We focus on ash from active volcanoes within the Aleutians, whose eruptions are likely to contribute Fe to the GoA. We assume the ash measured here should be broadly representative of volcanic ash compositions from this region. The Fe

isotopic composition of two fresh ash samples from Redoubt and Pavlof and six aged ash samples from Redoubt and Augustine—which represent the deposition of erupted ash over the past 8700 years—range from δ^{56}Fe = −0.01 to + 0.13‰ (Figure 2), which is within the range of previously published measurements of most igneous rocks.[18] The ash samples analyzed here contain quartz, plagioclase, and muscovite, although most of the ash particles are noncrystal-line, characterized as glass.[79] The aged ash may go through weak chemical weathering, as indicated by the increasing proportion of authigenic Fe hydroxides observed in the sequential leaching experiment for Fe.[43] There are no observable Fe isotopic fractionations between the fresh and aged ash, suggesting that chemical weathering is not a strong control on the observed isotopic composition. The Fe isotopic composition of both the fresh and aged volcanic ash endmember is close to the average upper continental crust composition and undergoes fractionation only during extreme secondary chemical weathering or diagenesis.

4.1.2. Wildfire Aerosols from Forest Fires. In this study, the bulk Fe isotopic compositions of two bulk natural wildfire aerosols were found to be δ^{56}Fe = −0.01 and +0.07‰ (Figure 2). Given the much higher content of Fe in the bedrock and soils of southcentral Alaska (~5% m/m), compared to the concentration of Fe in biomass (~50−150 μg g^{-1}),[80] the measured Fe isotopic signals of wildfire aerosols could plausibly be obscured by a large amount of Fe derived from the soil.[40] This highlights that the Fe isotopic signature of aerosols derived from biomass burning is close to the upper continental crust average and the flux of Fe from this process is dominated by the sediment contribution.

Early research on atmospheric aerosols from Bermuda suggested that low δ^{56}Fe values (δ^{56}Fe ≈ −0.5‰) may be derived from biomass burning.[81] A more recent study revealed the presence of suspended soil particles across all size fractions within the Fe-bearing atmospheric aerosol fraction during biomass burning events.[40] The average δ^{56}Fe values of soil, plants, and residual ash are δ^{56}Fe = +0.04, +0.08, and +0.09‰, respectively, suggesting minimal Fe isotopic fractionation during the process of biomass combustion and transformation of soil and vegetation to ash.[40]

4.1.3. Glaciofluvial Silts. Glaciofluvial silts are typically characterized by near-crustal δ^{56}Fe compositions (+0.07‰ to + 0.09‰) and should primarily reflect the contribution of particles and colloids derived from physical erosion, where the mechanical transport of lithogenic materials should proceed with minimal Fe isotope fractionation.[16,27,30,31] The Fe isotopic compositions of silts from eight rivers analyzed here have a restricted range (δ^{56}Fe = +0.02 to +0.12‰), similar to the average crustal values. These results are also broadly in accordance with observations of δ^{56}Fe measured in dissolved phases (<0.45 μm) from the Copper River glacial tributary system, which is also close to the crustal values (δ^{56}Fe = + 0.07‰).[27,31]

4.1.4. Dissolved Load. The δ^{56}Fe values in the dissolved load from glacial rivers in this study (−0.10 to + 0.04‰) span a narrow range close to the crustal composition, which may reflect the contribution of colloids derived from physical erosion with minimal isotopic fractionation from bedrock (Figure 3).[27] We observe a small offset between the measured δ^{56}Fe of suspended particulate matter and the dissolved loads (Figure 3), with the dissolved load being lighter than the suspended particulate matter by a mean value of 0.06 ±
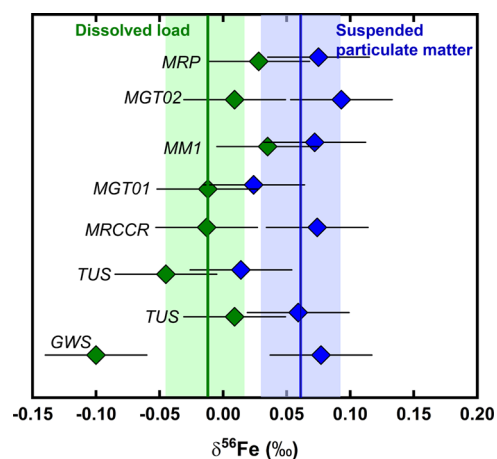
Figure 3. Fe isotopic compositions of paired glaciofluvial suspended particulate matter and dissolved load by sample location (see Table S1 for full sample names and locations). The solid lines represent the mean values. Error bars for Fe isotopic ratios determined in this study are long-term precision. The shaded area represents the 95% confidence intervals of the mean value.

0.031‰. A pattern of isotopically lighter dissolved phase (compared to the complimentary particulate phase) is also observed in glacially fed rivers in Greenland, where subglacial streams draining the Greenland ice sheet deliver a source of isotopically light dissolved Fe (average δ^{56}Fe ≈ −0.7‰) to the North Atlantic.[30] One possible reason for lower observed Fe isotope ratios of the dissolved load than silt is incongruent silicate weathering,[30,31] as this process is noted to drive subglacial stream Fe chemistry and may influence the δ^{56}Fe of dissolved Fe.

4.1.5. Loess. Previous studies on the Fe isotopic composition of loess-paleosol layers indicate nearly homoge-neous Fe isotopic compositions, regardless of variations in the major element composition.[18,26] As a result, fine-grained loess is often used to estimate the average composition of the upper continental crust.[26,82] In contrast to the uniform Fe isotopic compositions measured in previous loess profiles, the largest range in measured Fe isotopic compositions in this study is observed in the loess samples (δ^{56}Fe = −0.50 to +0.12‰, Figures 2 and 4), with the lighter Fe isotope compositions observed in both Chitina loess (<5 μm size fraction) and Kanakanak bluffs loess (<10 μm size fraction). The lightest Fe isotope composition (δ^{56}Fe = −0.32‰) in the Chitina loess section had the lowest Fe$_2$O$_3$ content in all loess samples (Fe$_2$O$_3$ = 7.6 wt %) and the highest LOI value (21 wt %).

As shown in Figure 4, the bottom layer in the Kanakanak bluff loess profile was characterized by the highest LOI value of 4.5 wt %, potentially indicating the presence of paleosols. We acknowledge that the loess samples analyzed here have likely been subject to many processes such as biological activity, chemical weathering, redox cycling and fluctuations, and water percolation/movement. Nevertheless, analysis of the Fe isotopic composition of several loess profiles allows us to determine the range in composition of this potential endmember to the GoA.

The LOI values in the top loess layers of the Kanakanak bluffs loess profile remain low (2.5−2.8 wt %), except for a small positive excursion (3.2 wt %) at the depth of 1.5 m, where the loess sample was characterized by a very fractionated Fe isotopic composition. The Fe isotope compositions of loess
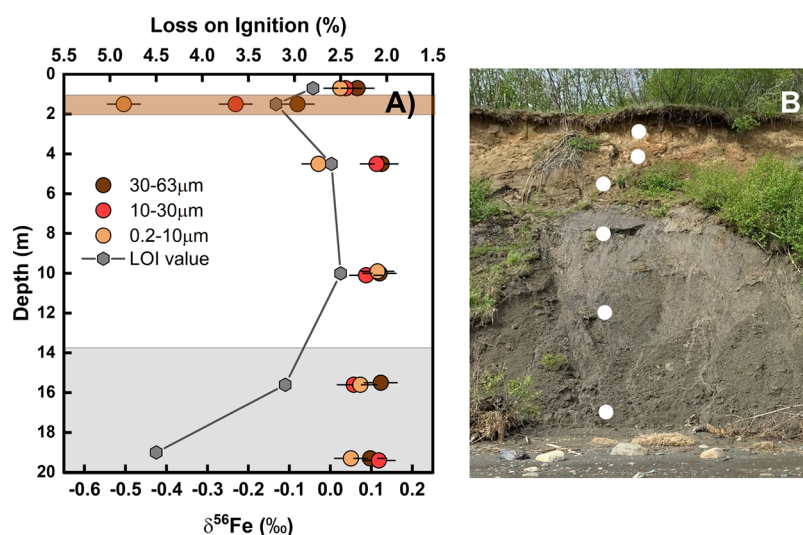
Figure 4. (A) Fe isotopic compositions of different size fractions (colored circles) and loss of ignition (LOI) values of loess (gray hexagons) from the Kanakanak bluffs, Alaska. The δ^{56}Fe isotopic compositions of three size fractions of loess were measured at six different depths. Error bars show the 95% confidence intervals. The lightest δ^{56}Fe values were observed at ~1.5 m depth, highlighted in brown in panel (A), where oxidized Fe may have accumulated. The light gray shaded area in panel (A) represents a possible paleosol layer, characterized by relatively high organic matter. The white circles in panel (B) represent the sample depths.

sampled from the Kanakanak bluffs profile do not show distinguishable fractionation with respect to sediment size, except for two samples. For these two samples, the large size fractions (10−30 and 30−63 μm) are characterized by δ^{56}Fe values closer to 0‰, while the smaller size fraction (0.2−10 μm) is characterized by isotopically lighter Fe isotopic composition of −0.23 and −0.50‰ respectively. One possible mechanism to explain this isotope fractionation is the preferential partial dissolution and later reprecipitation of Fe from the surface. In this scenario, a portion of the insoluble Fe(III) in the surface layer may be reduced to soluble Fe(II), moved down the loess profile through water percolation, and accumulated in an impermeable layer.[83] During this process, preferential removal of light Fe isotopes during partial dissolution could explain the distinct negative δ^{56}Fe value measured in this layer. This is consistent with field observations, where the lightest δ^{56}Fe values were observed in the finest fraction of the section highlighted in brown in Figure 4A, an area where the accumulation of Fe may have occurred.

4.2. Weathering Influence on Fe Isotopic Composition and Lability of Glacial Sediments. In glaciofluvial settings within Alaska, intense rates of physical weathering generate substantial quantities of fine-grained silts and clays, whose mineralogy typically reflects the mineralogy of the bulk bedrock.[41,84] In this study, the glacially derived Fe in suspended particulate matter and dissolved loads is not substantially fractionated by initial physical weathering. The suspended particulate matter has a range of δ^{56}Fe values from −0.02 to +0.09‰, whereas the dissolved load has slightly more negative δ^{56}Fe compositions which vary from −0.10 to +0.04‰, with average offset between these two classes being 0.06‰. Given that the glaciofluvial silts measured in this study span a narrow range in δ^{56}Fe values despite originating from a variety of bedrock compositional settings,[41,42] we suggest that processes other than bedrock composition are responsible for the large range of δ^{56}Fe values observed in the glaciogenic loess measured here.

Silicate dissolution during chemical weathering is a well-established mechanism for inducing Fe isotopic fractionation,[85,86] with experimental phyllosilicate and basalt dissolution initially releasing isotopically lighter Fe into solution with Fe isotopic fractionation between rock and solution (Δ^{56}Fe$_{solution-rock}$) as low as −1.20 to −1.80‰.[86,87] In this study, we observed distinct δ^{56}Fe variations in Kanakanak bluffs loess in different size fractions (Figure 4). Notably, the fine silt/clay fraction (<10 μm) exhibited significant Fe isotopic fractionation with δ^{56}Fe compositions as low as −0.50‰, in contrast to the larger grain size fraction, which had δ^{56}Fe compositions no lower than −0.08‰. The loess layer with fractionated Fe isotopic compositions was also characterized by a dark red color, potentially indicating the widespread presence of Fe(III)-(hydr)oxides. The Fe isotope fractionation coupled with secondary mineralization suggests mineral dissolution and Fe reprecipitation processes. Cycles of dissolution and precipitation during chemical weathering of continental material will result in an isotopically heavier residue and isotopically lighter Fe preferentially mobilized in the dissolved phase.[25] Due to the low solubility of Fe in oxic environments, dissolved Fe will rapidly reprecipitate as Fe(III)-hydroxides in the direct vicinity of primary minerals, resulting in secondary minerals with smaller grain sizes.[33,85] As a result, the small size fractions of sediments with high proportions of Fe(III)-hydroxides relative to the total Fe should be significantly enriched in isotopically light Fe.[85]

When this fine-grained, high surface-area-to-volume silicate material is transported to downstream environments by both aeolian and fluvial processes, additional chemical weathering occurs. Under typical chemical weathering conditions, soluble and mobile elements in sediments are depleted in the source material and transported to downstream environments, while less soluble and immobile elements are enriched in the parent material.[88,89] For example, aluminum (Al) is considered one of the relatively immobile elements during continental weathering, as it is incorporated into secondary clay minerals. In contrast, potassium (K) is highly mobile and is typically

depleted in soils.[90] High Al/K ratios in sediments are therefore considered to be indicative of chemical weathering.[90,91]

The phyllosilicate mineral chlorite is the dominant Fe-bearing mineral in both the loess and glaciofluvial silt samples from southcentral Alaska.[43] The isotopic fractionation during dissolution of chlorite may explain the isotopic variation observed in these loess samples during various stages of chemical weathering (Figure 5). The Al/K ratio correlates very
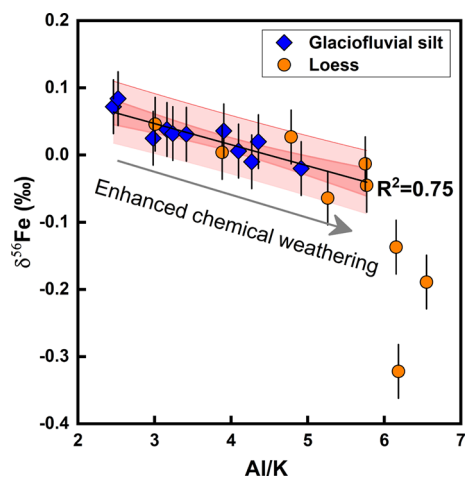
Figure 5. Stable Fe isotopic compositions of glaciofluvial silts and river valley loess (all <5 μm size fraction) correlated to Al/K mass ratios (m/m). Major element data are from Koffman et al.[43] Symbols are the same as in Figure 2. Error bars for iron isotopic ratios determined in this study are 95% confidence intervals. The black solid line is the best linear fit for Fe isotopes and Al/K ratio with a 95% confidence envelope (dark pink area) and 95% prediction envelope (light pink area) excluding three loess samples with particularly low δ^{56}Fe as these are hypothesized to have Fe fractionation due to the presence of organic carbon.

well with the δ^{56}Fe isotopic composition in the glaciofluvial silt and the loess samples studied here (Figure 5). At low Al/K values characteristic of early-stage chemical weathering, δ^{56}Fe values of glaciofluvial silt and loess are close to the crustal values, from −0.02 to +0.12‰, recording the δ^{56}Fe values of the bedrock they derived from. At high Al/K values which would indicate more intense rates of chemical weathering, glaciofluvial silt and loess are characterized by lighter δ^{56}Fe values from −0.32 to −0.06‰. Based on the relationship between Al/K ratios and δ^{56}Fe values, we hypothesize that the isotopic variability observed in our samples may be influenced by chemical weathering. The initial stages of chemical weathering either before or during transport would result in the dissolution of chlorite and other Fe-bearing minerals, with the release of isotopically lighter Fe during the dissolution, and subsequent precipitation as poorly crystalline Fe hydroxide minerals such as ferrihydrite and lepidocrocite in fine clays. As chemical weathering progresses, the fine clay proportion becomes more enriched in the light isotopes of Fe, which is consistent with the trends we observe with our data. This mechanism is supported by the ~14 times higher easily reducible Fe fraction found in the loess and glaciofluvial silt samples (median 2.3 ± 0.6 wt %) compared to fresh ash (0.16 ± 0.1 wt %),[43] as extracted by hydroxylamine hydrochloride. In sum, the correlation between Fe lability, degree of chemical weathering, and Fe isotopic composition supports the progressive weathering of primary Fe-bearing silicates to Fe

oxyhydroxides. However, the three samples with particularly low δ^{56}Fe do not correlate well with Al/K (Figure 5). It is unlikely that chemical weathering is the sole control on the large Fe isotopic fractionation observed in the loess samples. A range of processes, including biological activity, chemical weathering, redox cycling, and water movement could contribute to the Fe isotopic compositions as loess accumulated through time. For example, during the dissimilatory Fe reduction process, the δ^{56}Fe of Fe dissolved from a silicate soil mineral by siderophore-producing bacteria is as much as 0.8‰ lighter than bulk Fe in the mineral phase.[92] It is likely that the Fe isotopic composition of loess and other sedimentary archives such as permafrost will be similarly affected by multiple processes.

To further probe the influence of primary versus secondary minerals on observed Fe isotopic compositions, we conducted TEM measurements on a subset of samples. The Fe-bearing minerals present in the glaciofluvial silts were well-crystallized with a platy shape (Figure 6), and the lattice fringe of chlorite crystals was identified under high-resolution observation. The energy-dispersive X-ray spectroscopy data show peaks at Fe, Mg, Si, and O, and the lattice constant derived from the diffraction pattern is very close to that of chlorite, which is in good agreement with the published XRD measurements.[41,43] The Chitina loess samples with the lightest δ^{56}Fe compositions
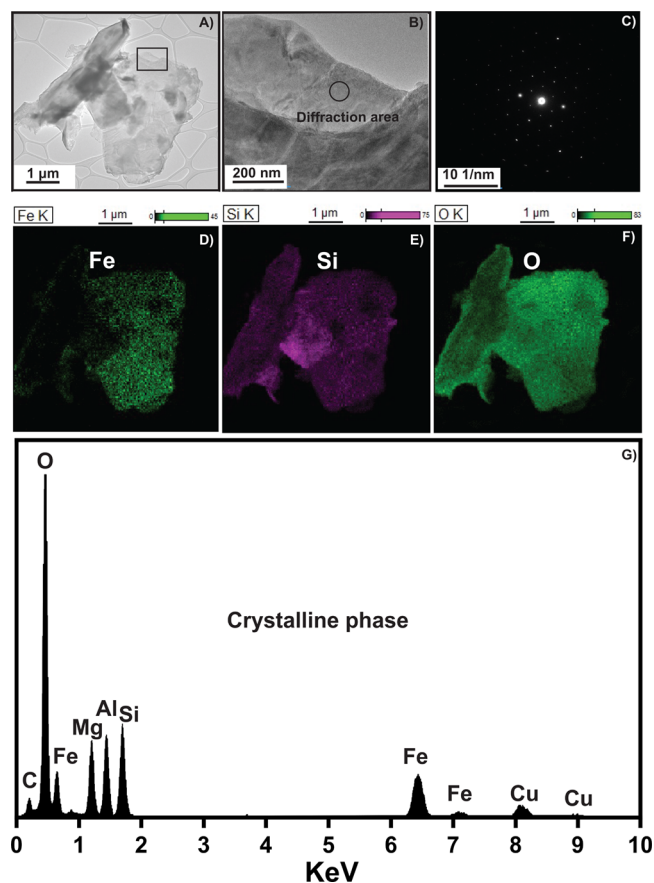
Figure 6. TEM images of well-crystallized Fe phases of a representative glaciofluvial silt sample AK2016-03 from Knik River in the <5 μm size fraction. TEM images (A,B) show ~1 μm clay particle sheets. The diffraction pattern in (C) shows that this particle is crystalline. X-ray spectra (D−G) show that it contains Fe, Mg, Si, and O within the crystalline structure.

contain two distinct types of Fe-bearing particles. The first type is a well-crystallized Fe silicate, similar to the Fe-bearing minerals observed in the glaciofluvial silt samples. The second type is Fe aggregates ranging in size from tens to hundreds of nanometers (Figure 7). The lack of crystal lattice fringes on
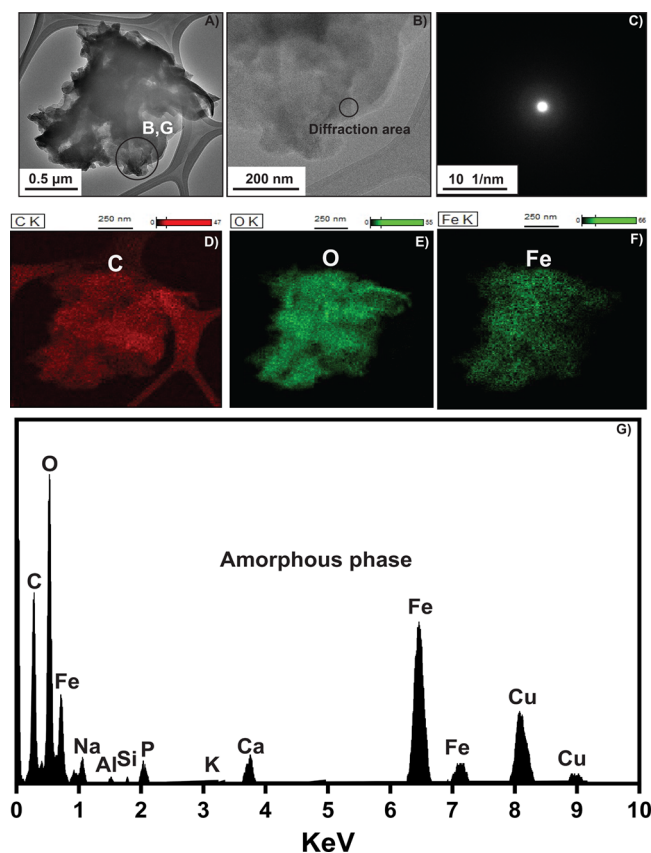
Figure 7. TEM images of amorphous Fe phases of a representative loess sample AK2016-13 from Chitina River in the <5 μm size fraction. TEM images (A, B) show ∼1 μm clay particles. The diffraction pattern in (C) shows that this particle is poorly crystalline or amorphous, and X-ray spectra (D−G) show that it contains Fe, Mg, C, and O within a poorly crystalline or amorphous structure.

these Fe particles (Figure 7B) and the diffraction pattern (Figure 7C) suggest that they are amorphous or poorly crystalline in nature. The X-ray spectral data show peaks at Fe and O, and no obvious peak at Si, indicating the presence of Fe-(hydr)oxides (Figure 7G). These poorly ordered Fe nanoparticulate aggregates, indicative of ferrihydrite, were widely observed in the loess samples, which revealed the widespread presence of these nanoparticles throughout the samples. Compared to the glaciofluvial silt, the significant presence of Fe-(hydr)oxides strongly suggests that the isotopic trends observed in the loess are related to the formation of the authigenic Fe-(hydr)oxides.

4.3. Influence of Organic Carbon on Fe Lability and Fe Isotopes in Loess.

The Fe in the loess is largely hosted in poorly crystalline Fe hydroxides and is correlated with the presence of organic carbon (Figure 7D, G). The biogeochemical cycling of Fe and carbon is strongly linked, with solid Fe shown to complex with and preserve organic carbon.[93] Studies have shown that more than 20% of organic carbon in sediments is bound to reactive Fe phases, with reactive Fe phases serving as a 'rusty sink' for organic carbon.[94] There is

evidence that organic carbon may have an inhibitory effect on the crystallization of ferric hydroxide, with experimental results suggesting that organic anions may disturb or even prevent the amorphous Fe-(hydr)oxides from further dehydration and crystallization.[95] In addition, dissolved organic carbon can be absorbed and coated to the surface of reactive Fe-(hydr)oxide particles, affecting their surface charge and adsorption behavior.[93,94,96] This sorption process involves strong complexation bonding between surface metals and acidic organic ligands, preventing further crystallization.[93] Given the substantial presence of amorphous Fe-(hydr)oxides in the loess samples analyzed here, the presence of organic carbon may play a role in maintaining the high Fe lability and reactivity of these mineral phases for the lifetime of sediment storage, which in the case of the loess may be upward of tens of thousands of years.

Combined evidence from the TEM imaging and Fe sequential extractions indicates the presence of reactive amorphous Fe-(hydr)oxides in the loess samples, whereas crystalline Fe oxides are rare. However, reactive Fe phases will become increasingly crystalline with time causing a decrease in their surface area, reactivity, and solubility.[97,98] Experimental work shows that crystallization of reactive amorphous Fe-(hydr)oxides to the minerals goethite or hematite is nearly complete after several years at room temperature,[99] which suggests that reactive amorphous Fe phases should be unstable in loess preserved for thousands of years. In contrast, we find an abundance of well-preserved amorphous Fe phases in our loess samples, which suggests the inhibition of crystallization of amorphous Fe-(hydr)oxides by organic carbon.

Iron isotopic compositions can provide valuable insights into the relationship between organic carbon and Fe phase transformation in aqueous systems.[92,100,101] Laboratory experiments show that organically complexed Fe extracted from Fe silicates is isotopically lighter than the primary Fe-bearing minerals.[92,101] These results are also consistent with the Fe isotopic behavior in streams, where carbon-bonded Fe is characterized by lighter Fe isotopic signatures.[27,30,31] For example, boreal-forested stream systems are characterized by much lower δ^{56}Fe values in the dissolved phase ranging down to δ^{56}Fe = −1.73 ‰ in the Copper River basin (Alaska) and correspond to high concentrations of dissolved organic carbon (DOC).[31] In this study, the correlation between the Fe isotopic composition of loess and LOI data highlights the potential association of labile Fe with organic carbon (Figure 8 and Table S4).

The liberation of Fe through chemical weathering and organic complexation has been invoked for observed Fe isotope fractionation during fluvial transport of sediments,[28,31,33,92,102] however discrepancies remain in the magnitude of the induced variability. A study of silicate soils developed on Gore Mountain (New York, USA) found that the δ^{56}Fe of Fe-organic complexation is as much as 0.8‰ lighter than bulk Fe measured in the unaltered minerals.[92] If Fe−C species indeed record the isotopic fractionation in the chemical weathering and organic complexation process, then the Fe isotopic composition of loess samples (<5 μm size fraction) should also be influenced by the fraction of Fe−C species. The isotope composition of Fe in loess (δ^{56}Fe$_{total}$) can be expressed as follows:

$$\delta^{56}\text{Fe}_{total} = \delta^{56}\text{Fe}_{\text{Fe}-\text{C}} \times f + \delta^{56}\text{Fe}_{residue} \times (1 - f) \qquad (2)$$
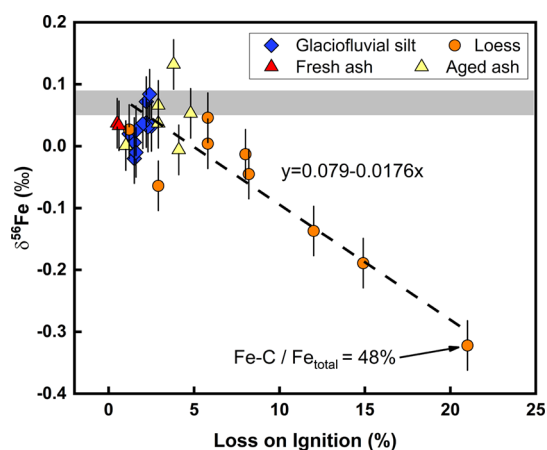
Figure 8. Variation of the δ^{56}Fe values of glaciofluvial silt, loess, and ash correlated to the LOI data. The gray bar represents the δ^{56}Fe values of upper continental crust.[29] The loess shown here is fine-grained ($<5\ \mu$m) from the river valley loess profiles.

where f is the fraction of organic carbon bonded Fe, δ^{56}Fe$_{Fe-C}$ is the isotopic composition of Fe in Fe–C species, and δ^{56}Fe$_{residue}$ is the isotopic composition of Fe in residue (nonorganically complexed) mineral phases. Based on the TEM imaging results, the residue mineral phases of loess are the primary silicate mineral phases, similar to the Fe-bearing phases of silts. Therefore, we estimate the δ^{56}Fe$_{residue}$ as the average upper continental crust value (δ^{56}Fe$_{residue}$ = +0.08‰).[26] The organic carbon content of loess can be linearly converted from the LOI data.[103] Assuming the fraction of organic carbon-bonded Fe is linearly related to the organic carbon content, then the value f can be expressed as follows:

$$f = \alpha \times \text{LOI} \tag{3}$$

where α is a constant described below. Therefore, the isotope composition of Fe in bulk loess should be linearly related to the LOI data and can be expressed with the following equation:

$$\delta^{56}\text{Fe}_{total} = \delta^{56}\text{Fe}_{Fe-C} \times \alpha \times \text{LOI} + \delta^{56}\text{Fe}_{residue} \times (1 - \alpha \times \text{LOI}) \tag{4}$$

Figure 8 illustrates the linear regression with LOI content and δ^{56}Fe values of loess samples. According to eqs 2 and 3, the intercept value of the linear regression line (δ^{56}Fe = +0.079‰) represents the isotopic composition of Fe in residual mineral phases, which is consistent with our assumption. For low LOI values the fraction of Fe–C species is lower, and the δ^{56}Fe$_{bulk}$ value of loess is largely controlled by the Fe isotopic composition of residual mineral phases. For high LOI values, the fraction of Fe–C in the sample is larger, and the δ^{56}Fe$_{bulk}$ value is more influenced by the fraction of Fe–C, which is derived from chemical weathering and organic complexation.

We now describe a method to estimate the isotopic fractionation between Fe–C phases and the original chlorite phases (the Δ^{56}Fe$_{Fe-C\text{-}Chlorite}$ value) in our Chitina loess. The sequential leaching results indicate that the Chitina loess sample with the lightest δ^{56}Fe$_{bulk}$ value (δ^{56}Fe = -0.32‰) has a reducible Fe fraction of 48%.[43] Assuming the reducible Fe fraction is entirely organic carbon-bonded, the resulting δ^{56}Fe$_{Fe-C}$ value and α in this sample can be calculated from eqs 2 and 3, giving δ^{56}Fe$_{Fe-C}$ = -0.73‰ and α = 2.29. This

calculated δ^{56}Fe$_{Fe-C}$ value is consistent with laboratory experimental results where the δ^{56}Fe isotopic composition of the organic complexation fraction on soil grains is lighter by $\sim$0.6–1‰ compared to Fe hosted in the mineral phases.[92]

While the approach described above successfully characterizes the observed relationships within our data, the calculations are for simplified circumstances. Eq 2 cannot explain any change in Fe sources or Fe isotopic fractionation in residual mineral phases. The calculations also do not consider other possible factors such as (i) not all the extracted Fe from the sodium dithionite leach experiment is complexed with organic carbon for the Chitina loess sample with the lightest δ^{56}Fe$_{bulk}$ value, which would result in an overestimate of the Fe–C fraction; (ii) kinetic isotopic fractionation during the organic carbon complexation process, or (iii) the Fe isotopic fractionation in intermediate Fe (II)$_{aq}$ and ferrihydrite phases during mineral dissolution (discussed in Section 4.2). Nonetheless, the model constrains the isotopic fractionation between Fe–C phases and the original chlorite phases.

Understanding and quantifying coupled Fe cycling and organic carbon stability is vital to predicting the composition, lability, and fate of sediment-bound Fe sources with respect to a changing climate. We demonstrate that there is an association of labile Fe with organic carbon, and this association is accompanied by a stable Fe isotopic fractionation likely due to Fe-organic complexation. As Fe isotope fractionation is ubiquitous in biogeochemical cycling, Fe isotopes can be a useful tool to investigate the transport and flux of Fe-bound organic carbon assuming that suspended particulate matter sourced from loess and/or permafrost retains its Fe isotopic composition during riverine transport to nearshore environments. For example, labile Fe that has been previously bound and preserved with organic carbon within a loess or permafrost bluff and subsequently released and transported to the riverine environment as a result of climate change-driven erosion should be detectable by a shift toward more negative Fe isotopic compositions of riverine suspended particulate matter. This would assume that sedimentary material not associated with organic carbon complexation and subject to physical and chemical weathering during erosion and riverine transport (e.g., glaciofluvial silt) retains a Fe isotopic composition close to the upper continental crust average (δ^{56}Fe$_{residue}$ = +0.08‰)[26] and is characterized by a lower proportion of easily reducible Fe compared to loess which has been noted in previous studies (e.g., Koffman et al.).[43] We, therefore, propose that Fe isotopic compositions may be a useful indicator of shifts in Fe sources and Fe lability to the nearshore environment. It is still unclear how the exposure and transport of this material affects the Fe lability and isotopic composition and warrants future study.

5. CONCLUSIONS

We measured the Fe isotopic compositions of several terrestrial sources that may contribute Fe to the Gulf of Alaska. Glaciofluvial river silts, wildfire aerosols, and fresh and aged volcanic ash have relatively constant δ^{56}Fe values regardless of geographical location and are similar to the composition of the upper continental crust. The Fe isotopic compositions of glaciogenic loess are not uniform, with the lowest δ^{56}Fe value observed in the Kanakanak bluffs loess profile which we attribute to post-depositional processes such as biological activity or water percolation. We found that loss on ignition, which is used as an indicator of organic carbon content, the

proportion of easily reducible Fe species, and Fe isotopic compositions covaried in loess samples. This indicates that bioavailable Fe is preserved in sedimentary archives in the presence of organic carbon and is characterized by a unique Fe isotopic signature. These results indicate that in some cases, Fe isotopes may be a useful proxy to trace the associations between organic carbon and Fe and to investigate the fate of organic carbon-bound Fe during redox cycling of Fe. While we lack constraints on the current flux of Fe sources to the Gulf of Alaska, we expect the bulk of material transported to the nearshore environment to be sourced from glaciofluvial silt. However, as climate change continues to accelerate in the subpolar environment, a new source of bioavailable Fe from organic-rich sedimentary archives such as loess or permafrost may become more significant and may be accompanied by a distinct lighter Fe isotopic composition of particulate matter in water.

ASSOCIATED CONTENT

Supporting Information

The Supporting Information is available free of charge at https://pubs.acs.org/doi/10.1021/acsearthspace-chem.3c00338.

> Additional details of sample sites, Fe isotopic data, Fe concentrations, results of Fe sequential leaching, LOI data, and reagents used for chemical processing (PDF)

> Fe isotopic composition with respect to the Fe content in glaciofluvial silt, loess, and volcanic ash (XLSX)

AUTHOR INFORMATION

Corresponding Author

Linqing Huang — *Scripps Institution of Oceanography, University of California San Diego, La Jolla, California 92093, United States;* orcid.org/0000-0002-7559-4881; Email: lih007@ucsd.edu

Authors

Sarah M. Aarons — *Scripps Institution of Oceanography, University of California San Diego, La Jolla, California 92093, United States;* orcid.org/0000-0002-3580-0820

Bess G. Koffman — *Department of Geology, Colby College, Waterville, Maine 04901, United States;* orcid.org/0000-0002-9451-4138

Wenhan Cheng — *College of Resources and Environment, Anhui Agricultural University, Hefei, Anhui 230036, China;* orcid.org/0000-0002-2832-2584

Lena Hanschka — *Department of Geology, Colby College, Waterville, Maine 04901, United States*

Lee Ann Munk — *Department of Geological Sciences, University of Alaska Anchorage, Anchorage, Alaska 99508, United States*

Jordan Jenckes — *Department of Chemistry, University of Alaska Anchorage, Anchorage, Alaska 99508, United States*

Emmet Norris — *Scripps Institution of Oceanography, University of California San Diego, La Jolla, California 92093, United States*

Carli A. Arendt — *Department of Marine, Earth and Atmospheric Sciences, North Carolina State University, Raleigh, North Carolina 27695, United States*

Complete contact information is available at:
https://pubs.acs.org/10.1021/acsearthspacechem.3c00338

REFERENCES

(1) Martin, J. H.; Fitzwater, S. E. Iron deficiency limits phytoplankton growth in the north-east Pacific subarctic. *Nature* **1988**, *331* (6154), 341−343.

(2) Charlson, R. J.; Lovelock, J. E.; Andreae, M. O.; Warren, S. G. Oceanic phytoplankton, atmospheric sulphur, cloud albedo and climate. *Nature* **1987**, *326* (6114), 655−661.

(3) Coale, K. H.; Johnson, K. S.; Chavez, F. P.; Buesseler, K. O.; Barber, R. T.; Brzezinski, M. A.; Cochlan, W. P.; Millero, F. J.; Falkowski, P. G.; Bauer, J. E. Southern Ocean iron enrichment experiment: carbon cycling in high-and low-Si waters. *Science* **2004**, *304* (5669), 408−414.

(4) Tagliabue, A.; Aumont, O.; Bopp, L. The impact of different external sources of iron on the global carbon cycle. *Geophys. Res. Lett.* **2014**, *41* (3), 920−926.

(5) Joos, F.; Sarmiento, J. L.; Siegenthaler, U. Estimates of the effect of Southern Ocean iron fertilization on atmospheric CO_2 concentrations. *Nature* **1991**, *349* (6312), 772−775.

(6) Martin, J. H.; Coale, K. H.; Johnson, K. S.; Fitzwater, S. E.; Gordon, R. M.; Tanner, S. J.; Hunter, C. N.; Elrod, V. A.; Nowicki, J. L.; Coley, T. L.; Barber, R. T.; Lindley, S.; Watson, A. J.; Van Scoy, K.; Law, C. S.; Liddicoat, M. I.; Ling, R.; Stanton, T.; Stockel, J.; Collins, C.; Anderson, A.; Bidigare, R.; Ondrusek, M.; Latasa, M.; Millero, F. J.; Lee, K.; Yao, W.; Zhang, J. Z.; Friederich, G.; Sakamoto, C.; Chavez, F.; Buck, K.; Kolber, Z.; Greene, R.; Falkowski, P.; Chisholm, S. W.; Hoge, F.; Swift, R.; Yungel, J.; Turner, S.; Nightingale, P.; Hatton, A.; Liss, P.; Tindale, N. W. Testing the iron hypothesis in ecosystems of the equatorial Pacific Ocean. *Nature* **1994**, *371* (6493), 123−129.

(7) Martínez-García, A.; Sigman, D. M.; Ren, H.; Anderson, R. F.; Straub, M.; Hodell, D. A.; Jaccard, S. L.; Eglinton, T. I.; Haug, G. H. Iron fertilization of the Subantarctic Ocean during the last ice age. *Science* **2014**, *343* (6177), 1347−1350.

(8) Conway, T. M.; Hamilton, D. S.; Shelley, R. U.; Aguilar-Islas, A. M.; Landing, W. M.; Mahowald, N. M.; John, S. G. Tracing and constraining anthropogenic aerosol iron fluxes to the North Atlantic Ocean using iron isotopes. *Nat. Commun.* **2019**, *10* (1), 2628.

(9) Kurisu, M.; Takahashi, Y.; Iizuka, T.; Uematsu, M. Very low isotope ratio of iron in fine aerosols related to its contribution to the surface ocean. *J. Geophys. Res.: Atmos.* **2016**, *121* (18), 11119−11136.

(10) Weis, J.; Schallenberg, C.; Chase, Z.; Bowie, A. R.; Wojtasiewicz, B.; Perron, M. M.; Mallet, M. D.; Strutton, P. G. Southern Ocean phytoplankton stimulated by wildfire emissions and sustained by iron recycling. *Geophys. Res. Lett.* **2022**, *49* (11), No. e2021GL097538.

(11) Kramer, S. J.; Bisson, K. M.; Mitchell, C. What data are needed to detect wildfire effects on coastal ecosystems? A case study during the Thomas Fire. *Front. Mar. Sci.* **2023**, *10*, No. 1267681, DOI: 10.3389/fmars.2023.1267681.

(12) Rout, G. R.; Sahoo, S. Role of iron in plant growth and metabolism. *Reviews in Agricultural Science* **2015**, *3*, 1–24.

(13) Nealson, K. H.; Saffarini, D. Iron and manganese in anaerobic respiration: environmental significance, physiology, and regulation. *Annual review of microbiology* **1994**, *48*, 311–344.

(14) Mark Moore, C.; Mills, M. M.; Achterberg, E. P.; Geider, R. J.; LaRoche, J.; Lucas, M. I.; McDonagh, E. L.; Pan, X.; Poulton, A. J.; Rijkenberg, M. J. Large-scale distribution of Atlantic nitrogen fixation controlled by iron availability. *Nat. Geosci.* **2009**, *2* (12), 867–871.

(15) Crusius, J.; Schroth, A. W.; Resing, J. A.; Cullen, J.; Campbell, R. W. Seasonal and spatial variabilities in northern Gulf of Alaska surface water iron concentrations driven by shelf sediment resuspension, glacial meltwater, a Yakutat eddy, and dust. *Global Biogeochemical Cycles* **2017**, *31* (6), 942–960.

(16) Dauphas, N.; John, S. G.; Rouxel, O. Iron isotope systematics. *Reviews in Mineralogy and Geochemistry* **2017**, *82* (1), 415–510.

(17) Weyer, S.; Anbar, A. D.; Brey, G. P.; Münker, C.; Mezger, K.; Woodland, A. B. Iron isotope fractionation during planetary differentiation. *Earth and Planetary Science Letters* **2005**, *240* (2), 251–264.

(18) Beard, B. L.; Johnson, C. M.; Skulan, J. L.; Nealson, K. H.; Cox, L.; Sun, H. Application of Fe isotopes to tracing the geochemical and biological cycling of Fe. *Chem. Geol.* **2003**, *195* (1–4), 87–117.

(19) Teng, F.-Z.; Dauphas, N.; Helz, R. T. Iron isotope fractionation during magmatic differentiation in Kilauea Iki lava lake. *Science* **2008**, *320* (5883), 1620–1622.

(20) Poitrasson, F.; Halliday, A. N.; Lee, D.-C.; Levasseur, S.; Teutsch, N. Iron isotope differences between Earth, Moon, Mars and Vesta as possible records of contrasted accretion mechanisms. *Earth and Planetary Science Letters* **2004**, *223* (3–4), 253–266.

(21) Fitzsimmons, J. N.; Conway, T. M. Novel insights into marine iron biogeochemistry from iron isotopes. *Annual Review of Marine Science* **2023**, *15*, 383–406.

(22) Conway, T. M.; John, S. G. Quantification of dissolved iron sources to the North Atlantic Ocean. *Nature* **2014**, *511* (7508), 212–215.

(23) Fitzsimmons, J. N.; Carrasco, G. G.; Wu, J.; Roshan, S.; Hatta, M.; Measures, C. I.; Conway, T. M.; John, S. G.; Boyle, E. A. Partitioning of dissolved iron and iron isotopes into soluble and colloidal phases along the GA03 GEOTRACES North Atlantic Transect. *Deep Sea Research Part II: Topical Studies in Oceanography* **2015**, *116*, 130–151.

(24) Kurisu, M.; Sakata, K.; Uematsu, M.; Ito, A.; Takahashi, Y. Contribution of combustion Fe in marine aerosols over the northwestern Pacific estimated by Fe stable isotope ratios. *Atmospheric Chemistry and Physics* **2021**, *21* (20), 16027–16050.

(25) Fantle, M. S.; DePaolo, D. J. Iron isotopic fractionation during continental weathering. *Earth and Planetary Science Letters* **2004**, *228* (3–4), 547–562.

(26) Poitrasson, F. On the iron isotope homogeneity level of the continental crust. *Chem. Geol.* **2006**, *235* (1–2), 195–200.

(27) Escoube, R.; Rouxel, O. J.; Pokrovsky, O. S.; Schroth, A.; Holmes, R. M.; Donard, O. F. Iron isotope systematics in Arctic rivers. *C. R. Geosci.* **2015**, *347* (7–8), 377–385.

(28) Hirst, C.; Andersson, P. S.; Kooijman, E.; Schmitt, M.; Kutscher, L.; Maximov, T.; Mörth, C.-M.; Porcelli, D. Iron isotopes reveal the sources of Fe-bearing particles and colloids in the Lena River basin. *Geochim. Cosmochim. Acta* **2020**, *269*, 678–692.

(29) Raiswell, R.; Tranter, M.; Benning, L. G.; Siegert, M.; De'ath, R.; Huybrechts, P.; Payne, T. Contributions from glacially derived sediment to the global iron (oxyhydr) oxide cycle: Implications for iron delivery to the oceans. *Geochim. Cosmochim. Acta* **2006**, *70* (11), 2765–2780.

(30) Stevenson, E. I.; Fantle, M. S.; Das, S. B.; Williams, H. M.; Aciego, S. M. The iron isotopic composition of subglacial streams

draining the Greenland ice sheet. *Geochim. Cosmochim. Acta* **2017**, *213*, 237–254.

(31) Schroth, A. W.; Crusius, J.; Chever, F.; Bostick, B. C.; Rouxel, O. J. Glacial influence on the geochemistry of riverine iron fluxes to the Gulf of Alaska and effects of deglaciation. *Geophys. Res. Lett.* **2011**, *38* (16), L048367 DOI: 10.1029/2011GL048367.

(32) De Jong, J.; Schoemann, V.; Tison, J.-L.; Becquevort, S.; Masson, F.; Lannuzel, D.; Petit, J.; Chou, L.; Weis, D.; Mattielli, N. Precise measurement of Fe isotopes in marine samples by multi-collector inductively coupled plasma mass spectrometry (MC-ICP-MS). *Anal. Chim. Acta* **2007**, *589* (1), 105–119.

(33) Hirst, C.; Andersson, P. S.; Shaw, S.; Burke, I. T.; Kutscher, L.; Murphy, M. J.; Maximov, T.; Pokrovsky, O. S.; Mörth, C.-M.; Porcelli, D. Characterisation of Fe-bearing particles and colloids in the Lena River basin, NE Russia. *Geochim. Cosmochim. Acta* **2017**, *213*, 553–573.

(34) Ilina, S. M.; Poitrasson, F.; Lapitskiy, S. A.; Alekhin, Y. V.; Viers, J.; Pokrovsky, O. S. Extreme iron isotope fractionation between colloids and particles of boreal and temperate organic-rich waters. *Geochim. Cosmochim. Acta* **2013**, *101*, 96–111.

(35) Kurisu, M.; Sakata, K.; Miyamoto, C.; Takaku, Y.; Iizuka, T.; Takahashi, Y. Variation of iron isotope ratios in anthropogenic materials emitted through combustion processes. *Chem. Lett.* **2016**, *45* (8), 970–972.

(36) Wang, Y.; Chen, H.-H.; Tang, R.; He, D.; Lee, Z.; Xue, H.; Wells, M.; Boss, E.; Chai, F. Australian fire nourishes ocean phytoplankton bloom. *Sci. Total Environ.* **2022**, *807*, No. 150775.

(37) Myriokefalitakis, S.; Ito, A.; Kanakidou, M.; Nenes, A.; Krol, M. C.; Mahowald, N. M.; Scanza, R. A.; Hamilton, D. S.; Johnson, M. S.; Meskhidze, N. Reviews and syntheses: the GESAMP atmospheric iron deposition model intercomparison study. *Biogeosciences* **2018**, *15* (21), 6659–6684.

(38) Guelke, M.; Von Blanckenburg, F. Fractionation of stable iron isotopes in higher plants. *Environmental science & technology* **2007**, *41* (6), 1896–1901.

(39) von Blanckenburg, F.; von Wirén, N.; Guelke, M.; Weiss, D. J.; Bullen, T. D. Fractionation of metal stable isotopes by higher plants. *Elements* **2009**, *5* (6), 375–380.

(40) Kurisu, M.; Takahashi, Y. Testing iron stable isotope ratios as a signature of biomass burning. *Atmosphere* **2019**, *10* (2), 76.

(41) Muhs, D. R.; Budahn, J. R.; McGeehin, J. P.; Bettis, E. A., III; Skipp, G.; Paces, J. B.; Wheeler, E. A. Loess origin, transport, and deposition over the past 10,000 years, Wrangell-St. Elias National Park, Alaska. *Aeolian Research* **2013**, *11*, 85–99.

(42) Muhs, D. R.; McGeehin, J. P.; Beann, J.; Fisher, E. Holocene loess deposition and soil formation as competing processes, Matanuska Valley, southern Alaska. *Quat. Res.* **2004**, *61* (3), 265–276.

(43) Koffman, B. G.; Yoder, M. F.; Methven, T.; Hanschka, L.; Sears, H. B.; Saylor, P. L.; Wallace, K. L. Glacial dust surpasses both volcanic ash and desert dust in its iron fertilization potential. *Global Biogeochem. Cycles* **2021**, *35*, No. e2020GB006821.

(44) Crusius, J.; Schroth, A. W.; Gassó, S.; Moy, C. M.; Levy, R. C.; Gatica, M. Glacial flour dust storms in the Gulf of Alaska: Hydrologic and meteorological controls and their importance as a source of bioavailable iron. *Geophys. Res. Lett.* **2011**, *38* (6), L046573 DOI: 10.1029/2010GL046573.

(45) Journet, E.; Desboeufs, K. V.; Caquineau, S.; Colin, J. L. Mineralogy as a critical factor of dust iron solubility. *Geophys. Res. Lett.* **2008**, *35* (7), L031589 DOI: 10.1029/2007GL031589.

(46) Muhs, D. R.; Bettis, E.; Chan, M.; Archer, A. Quaternary loess-paleosol sequences as examples of climate-driven sedimentary extremes. *Geol. Soc. Am.* **2003**, *370*, 53–74.

(47) Lea, P. D. Pleistocene periglacial eolian deposits in southwestern Alaska; sedimentary facies and depositional processes. *J. Sediment. Res.* **1990**, *60* (4), 582–591.

(48) Bhatia, M. P.; Kujawinski, E. B.; Das, S. B.; Breier, C. F.; Henderson, P. B.; Charette, M. A. Greenland meltwater as a significant and potentially bioavailable source of iron to the ocean. *Nature Geoscience* **2013**, *6* (4), 274–278.

(49) Arendt, C. A.; Aciego, S. M.; Sims, K. W.; Robbins, M. Sequential separation of uranium, hafnium and neodymium from natural waters concentrated by iron coprecipitation. *Geostandards and Geoanalytical Research* **2015**, *39* (3), 293−303.

(50) Browning, T. J.; Bouman, H. A.; Henderson, G. M.; Mather, T. A.; Pyle, D. M.; Schlosser, C.; Woodward, E. M. S.; Moore, C. M. Strong responses of Southern Ocean phytoplankton communities to volcanic ash. *Geophys. Res. Lett.* **2014**, *41* (8), 2851−2857.

(51) Simonella, L. E.; Palomeque, M.; Croot, P.; Stein, A.; Kupczewski, M.; Rosales, A.; Montes, M. L.; Colombo, F.; Garcia, M. G.; Villarosa, G. Soluble iron inputs to the Southern Ocean through recent andesitic to rhyolitic volcanic ash eruptions from the Patagonian Andes. *Global Biogeochem. Cycles* **2015**, *29* (8), 1125−1144.

(52) Duggen, S.; Olgun, N.; Croot, P.; Hoffmann, L.; Dietze, H.; Delmelle, P.; Teschner, C. The role of airborne volcanic ash for the surface ocean biogeochemical iron-cycle: a review. *Biogeosciences* **2010**, *7* (3), 827−844.

(53) Luo, M.; Torres, M. E.; Hong, W.-L.; Pape, T.; Fronzek, J.; Kutterolf, S.; Mountjoy, J. J.; Orpin, A.; Henkel, S.; Huhn, K. Impact of iron release by volcanic ash alteration on carbon cycling in sediments of the northern Hikurangi margin. *Earth Planet. Sci. Lett.* **2020**, *541*, No. 116288.

(54) Schneider, D. J.; Van Eaton, A. R.; Wallace, K. L. Satellite observations of the 2016−2017 eruption of Bogoslof volcano: aviation and ash fallout hazard implications from a water-rich eruption. *Bull. Volcanol.* **2020**, *82* (3), 29.

(55) Duggen, S.; Croot, P.; Schacht, U.; Hoffmann, L. Subduction zone volcanic ash can fertilize the surface ocean and stimulate phytoplankton growth: Evidence from biogeochemical experiments and satellite data. *Geophys. Res. Lett.* **2007**, *34* (1), L027522 DOI: 10.1029/2006GL027522.

(56) Frogner, P.; Gíslason, S. R.; Oskarsson, N. Fertilizing potential of volcanic ash in ocean surface water. *Geology* **2001**, *29* (6), 487−490.

(57) Bisson, K.; Gassó, S.; Mahowald, N.; Wagner, S.; Koffman, B.; Carn, S.; Deutsch, S.; Gazel, E.; Kramer, S.; Krotkov, N. Observing ocean ecosystem responses to volcanic ash. *Remote Sens. Environ.* **2023**, *296*, No. 113749.

(58) Hamme, R. C.; Webley, P. W.; Crawford, W. R.; Whitney, F. A.; DeGrandpre, M. D.; Emerson, S. R.; Eriksen, C. C.; Giesbrecht, K. E.; Gower, J. F.; Kavanaugh, M. T. Volcanic ash fuels anomalous plankton bloom in subarctic northeast Pacific. *Geophys. Res. Lett.* **2010**, *37* (19), L044629 DOI: 10.1029/2010GL044629.

(59) Langmann, B.; Zakšek, K.; Hort, M.; Duggen, S. Volcanic ash as fertiliser for the surface ocean. *Atmospheric Chemistry and Physics* **2010**, *10* (8), 3891−3899.

(60) Flower, V. J.; Kahn, R. A. Assessing the altitude and dispersion of volcanic plumes using MISR multi-angle imaging from space: Sixteen years of volcanic activity in the Kamchatka Peninsula, Russia. *Journal of Volcanology and Geothermal Research* **2017**, *337*, 1−15.

(61) Till, A. B.; Yount, M.; Bevier, M. The geologic history of Redoubt volcano, Alaska. *Journal of volcanology and geothermal research* **1994**, *62* (1−4), 11−30.

(62) Tang, W.; Llort, J.; Weis, J.; Perron, M. M.; Basart, S.; Li, Z.; Sathyendranath, S.; Jackson, T.; Sanz Rodriguez, E.; Proemse, B. C.; et al. Widespread phytoplankton blooms triggered by 2019−2020 Australian wildfires. *Nature* **2021**, *597* (7876), 370−375.

(63) Revels, B. N.; Zhang, R.; Adkins, J. F.; John, S. G. Fractionation of iron isotopes during leaching of natural particles by acidic and circumneutral leaches and development of an optimal leach for marine particulate iron isotopes. *Geochim. Cosmochim. Acta* **2015**, *166*, 92−104.

(64) Poulton, S. W.; Canfield, D. E. Development of a sequential extraction procedure for iron: implications for iron partitioning in continentally derived particulates. *Chemical geology* **2005**, *214* (3−4), 209−221.

(65) Chester, R.; Hughes, M. A chemical technique for the separation of ferro-manganese minerals, carbonate minerals and adsorbed trace elements from pelagic sediments. *Chemical geology* **1967**, *2*, 249−262.

(66) Heron, G.; Crouzet, C.; Bourg, A. C.; Christensen, T. H. Speciation of Fe (II) and Fe (III) in contaminated aquifer sediments using chemical extraction techniques. *Environmental science & technology* **1994**, *28* (9), 1698−1705.

(67) Mehra, O.; Jackson, M., Iron oxide removal from soils and clays by a dithionite−citrate system buffered with sodium bicarbonate. In *Clays and clay minerals*; Elsevier: 2013; pp 317-327.

(68) Raiswell, R.; Canfield, D.; Berner, R. A comparison of iron extraction methods for the determination of degree of pyritisation and the recognition of iron-limited pyrite formation. *Chemical geology* **1994**, *111* (1−4), 101−110.

(69) Koffman, B. G.; Goldstein, S. L.; Winckler, G.; Borunda, A.; Kaplan, M. R.; Bolge, L.; Cai, Y.; Recasens, C.; Koffman, T. N. B.; Vallelonga, P. New Zealand as a source of mineral dust to the atmosphere and ocean. *Quaternary Science Reviews* **2021**, *251*, No. 106659.

(70) Bokhari, S. N. H.; Meisel, T. C. Method development and optimization of sodium peroxide sintering for geological samples. *Geostandards and Geoanalytical Research* **2017**, *41* (2), 181−195.

(71) An, Y.; Huang, J.-X.; Griffin, W.; Liu, C.; Huang, F. Isotopic composition of Mg and Fe in garnet peridotites from the Kaapvaal and Siberian cratons. *Geochim. Cosmochim. Acta* **2017**, *200*, 167−185.

(72) Huang, F.; Zhang, Z.; Lundstrom, C. C.; Zhi, X. Iron and magnesium isotopic compositions of peridotite xenoliths from Eastern China. *Geochim. Cosmochim. Acta* **2011**, *75* (12), 3318−3334.

(73) Dauphas, N.; Rouxel, O. Mass spectrometry and natural variations of iron isotopes. *Mass Spectrometry Reviews* **2006**, *25* (4), 515−550.

(74) Craddock, P. R.; Dauphas, N. Iron isotopic compositions of geological reference materials and chondrites. *Geostandards and Geoanalytical Research* **2011**, *35* (1), 101−123.

(75) Dauphas, N.; Pourmand, A.; Teng, F.-Z. Routine isotopic analysis of iron by HR-MC-ICPMS: How precise and how accurate? *Chem. Geol.* **2009**, *267* (3−4), 175−184.

(76) Kim, S.; Liu, G.; Minor, A. M. FIB Sample Preparation of Polymer Thin Films on Hard Substrates Using the Shadow-FIB Method. *Microscopy Today* **2009**, *17* (6), 20−23.

(77) Johnson, C.; Beard, B.; Weyer, S. *Iron geochemistry: an isotopic perspective*; Springer: 2020.

(78) Longman, J.; Dunlea, A. G.; Böning, P.; Palmer, M. R.; Gernon, T. M.; McManus, J.; Manners, H. R.; Homoky, W. B.; Pahnke, K. Release of tephra-hosted iron during early diagenesis fingerprinted by iron isotopes. *Earth and planetary science letters* **2023**, *605*, No. 118016.

(79) Ayris, P.; Delmelle, P. Volcanic and atmospheric controls on ash iron solubility: A review. *Physics and Chemistry of the Earth, Parts A/B/C* **2012**, *45*, 103−112.

(80) Hänsch, R.; Mendel, R. R. Physiological functions of mineral micronutrients (cu, Zn, Mn, Fe, Ni, Mo, B, cl). *Current opinion in plant biology* **2009**, *12* (3), 259−266.

(81) Mead, C.; Herckes, P.; Majestic, B. J.; Anbar, A. D. Source apportionment of aerosol iron in the marine environment using iron isotope analysis. *Geophys. Res. Lett.* **2013**, *40* (21), 5722−5727.

(82) Gong, Y.; Xia, Y.; Huang, F.; Yu, H. Average iron isotopic compositions of the upper continental crust: constrained by loess from the Chinese Loess Plateau. *Acta Geochimica* **2017**, *36*, 125−131.

(83) Qi, Y.-H.; Cheng, W.; Nan, X.-Y.; Yang, F.; Li, J.; Li, D.-C.; Lundstrom, C. C.; Yu, H.-M.; Zhang, G.-L.; Huang, F. Iron stable isotopes in bulk soil and sequential extracted fractions trace Fe redox cycling in paddy soils. *J. Agric. Food Chem.* **2020**, *68* (31), 8143−8150.

(84) Anderson, S. P. Glaciers show direct linkage between erosion rate and chemical weathering fluxes. *Geomorphology* **2005**, *67* (1−2), 147−157.

(85) Kiczka, M.; Wiederhold, J. G.; Frommer, J.; Voegelin, A.; Kraemer, S. M.; Bourdon, B.; Kretzschmar, R. Iron speciation and isotope fractionation during silicate weathering and soil formation in

an alpine glacier forefield chronosequence. *Geochim. Cosmochim. Acta* **2011**, *75* (19), 5559−5573.

(86) Kiczka, M.; Wiederhold, J. G.; Frommer, J.; Kraemer, S. M.; Bourdon, B.; Kretzschmar, R. Iron isotope fractionation during proton- and ligand-promoted dissolution of primary phyllosilicates. *Geochim. Cosmochim. Acta* **2010**, *74* (11), 3112−3128.

(87) Chapman, J. B.; Weiss, D. J.; Shan, Y.; Lemburger, M. Iron isotope fractionation during leaching of granite and basalt by hydrochloric and oxalic acids. *Geochim. Cosmochim. Acta* **2009**, *73* (5), 1312−1324.

(88) Nesbitt, H.; Young, G. Prediction of some weathering trends of plutonic and volcanic rocks based on thermodynamic and kinetic considerations. *Geochimica et cosmochimica acta* **1984**, *48* (7), 1523−1534.

(89) Yang, S.; Li, C.; Yang, D.; Li, X. Chemical weathering of the loess deposits in the lower Changjiang Valley, China, and paleoclimatic implications. *Quaternary International* **2004**, *117* (1), 27−34.

(90) Condie, K. C.; Dengate, J.; Cullers, R. L. Behavior of rare earth elements in a paleoweathering profile on granodiorite in the Front Range, Colorado, USA. *Geochim. Cosmochim. Acta* **1995**, *59* (2), 279−294.

(91) Bayon, G.; Burton, K.; Soulet, G.; Vigier, N.; Dennielou, B.; Etoubleau, J.; Ponzevera, E.; German, C.; Nesbitt, R. Hf and Nd isotopes in marine sediments: Constraints on global silicate weathering. *Earth and Planetary Science Letters* **2009**, *277* (3−4), 318−326.

(92) Brantley, S. L.; Liermann, L.; Bullen, T. D. Fractionation of Fe isotopes by soil microbes and organic acids. *Geology* **2001**, *29* (6), 535−538.

(93) Kaiser, K.; Guggenberger, G. The role of DOM sorption to mineral surfaces in the preservation of organic matter in soils. *Organic geochemistry* **2000**, *31* (7−8), 711−725.

(94) Lalonde, K.; Mucci, A.; Ouellet, A.; Gélinas, Y. Preservation of organic matter in sediments promoted by iron. *Nature* **2012**, *483* (7388), 198−200.

(95) Schwertmann, U. Inhibitory effect of soil organic matter on the crystallization of amorphous ferric hydroxide. *Nature* **1966**, *212* (5062), 645−646.

(96) Perret, D.; Gaillard, J.-F.; Dominik, J.; Atteia, O. The diversity of natural hydrous iron oxides. *Environmental science & technology* **2000**, *34* (17), 3540−3546.

(97) Schwertmann, U.; Taylor, R. M. Iron oxides. *Minerals in soil environments* **2018**, *1*, 379−438.

(98) Bigham, J.; Golden, D.; Bowen, L.; Buol, S.; Weed, S. Iron Oxide Mineralogy of Well-drained Ultisols and Oxisols: I. Characterization of Iron Oxides in Soil Clays by Mössbauer Spectroscopy, X-ray Diffractometry, and Selected Chemical Techniques. *Soil Science Society of America Journal* **1978**, *42* (5), 816−825.

(99) Schwertmann, U.; Murad, E. Effect of pH on the formation of goethite and hematite from ferrihydrite. *Clays and Clay Minerals* **1983**, *31*, 277−284.

(100) Beard, B. L.; Johnson, C. M.; Cox, L.; Sun, H.; Nealson, K. H.; Aguilar, C. Iron isotope biosignatures. *Science* **1999**, *285* (5435), 1889−1892.

(101) Brantley, S. L.; Liermann, L. J.; Guynn, R. L.; Anbar, A.; Icopini, G. A.; Barling, J. Fe isotopic fractionation during mineral dissolution with and without bacteria. *Geochim. Cosmochim. Acta* **2004**, *68* (15), 3189−3204.

(102) Ingri, J.; Malinovsky, D.; Rodushkin, I.; Baxter, D. C.; Widerlund, A.; Andersson, P.; Gustafsson, Ö.; Forsling, W.; Öhlander, B. Iron isotope fractionation in river colloidal matter. *Earth and Planetary Science Letters* **2006**, *245* (3−4), 792−798.

(103) Konen, M. E.; Jacobs, P. M.; Burras, C. L.; Talaga, B. J.; Mason, J. A. Equations for predicting soil organic carbon using loss-on-ignition for north central US soils. *Soil science society of America journal* **2002**, *66* (6), 1878−1881.